Quantitative x-ray microscopic analysis of individual thermoresponsive microgel particles in aqueous solution

Birgit A. Graf-Zeiler[1], Andreas Späth[1], Gaio Paradossi[2], Shivkumar Ghugare[2,3], George Tzvetkov[4], Rainer H. Fink[1,5]

[1] Physikalische Chemie II and ICMM, Friedrich-Alexander-Universität Erlangen-Nürnberg (FAU), Egerlandstraße 3, 91058 Erlangen, Germany

[2] Dipartimento di Scienze e Tecnologie Chimiche, Università di Roma Tor Vergata, Via della Ricerca Scientifica, 00133 Roma, Italy

[3] present address: Solvay Research & Innovation Centre, Plot no. 72/73/74, Alindra Extention, G.I.D.C. Estate, Savli, Dist. Vadadora, 391770 Gujarat, India

[4] Department of Inorganic Chemistry, Faculty of Chemistry, University of Sofia, James Bourchier 1, 1164 Sofia, Bulgaria

[5] CENEM, Friedrich-Alexander Universität Erlangen-Nürnberg, Egerlandstraße 3, 91058 Erlangen, Germany

Abstract

High resolution scanning soft X-ray transmission microscopy (STXM) has been employed to investigate individual thermoresponsive microgel particles in aqueous environment. STXM generates 2-dimensional projections with spatial resolutions in the regime of few 10 nm. In the present study we are able to regain the 3D structure of the investigated specimen and observe the deswelling of the microgel particles upon heating, thus offering insight into the thermoresponsive behaviour of individual differently sized particles. We employ a 2-shell model that is able to derive the radial concentration profile of individual microgels particles and thus serves as a complementary method to scattering experiments that average over all particles. Furthermore, we are able to detect the different deswelling behaviour of the particle interior and its interface to the water environment.

1. Introduction

Microgels are suspensions of colloidal polymer networks incorporating a significant solvent content and with particle diameters ranging from 100 nm to some micrometers [1-4]. The swelling behaviour and related size of microgel particles can be influenced by external stimuli that unbalance the osmotic equilibrium of the particles and their solvent matrix resulting in switchable properties of the suspension [5-8]. The most investigated stimuli for swelling and deswelling in microgel particles are temperature and pH [6,9-11]. Switchable microgels have been investigated aiming on various fields of application, such as drug delivery with controllable release [12-15], separation processes [16], sensors [17-19] or biotechnology [20-22]. Composites of microgels and inorganic nanoparticles offer a broad range of unique properties [7,23-25]. Microgel suspensions are very resistant to aggregation, since the polymer particles usually carry covalently bound charged groups that also determine the electrophoresis properties of the gel [6,26,27]. Furthermore, these systems can be non-toxic,

non-carcinogenic and biocompatible. The most intensely studied thermoresponsive microgels are those containing poly(*N*-isopropylacrylamide) (PNIPAM) [7,8,28-31]. Below the volume phase transition temperature (VPTT) of 32°C PNIPAM microgel particles consist of a loose network of cross-linked polymer chains with a comparably high solvent content and dangling surface chains. Above the VPTT the PNIPAM chains coil up, the particles deswell and the solvent is mainly released due to energetically more favourable internal interactions within the polymer network [31-33]. The result is a temperature dependent change in optical and mechanical properties of the microgel [7,8,31,34] and a strong thermophoretic effect [35,36].

Analytical *in-situ* studies of microgel swelling and deswelling are mainly performed by means of dynamic light scattering (DLS) or small-angle neutron scattering (SANS) [7,29,37]. While these techniques enable the determination of average particle diameters with high resolution and especially directly in solution (in contrast to, e.g., electron microscopy), it is not possible to investigate individual particles. Therefore these techniques are especially useful for highly monodisperse microgels and with a homogeneous swelling behaviour (i.e., homogeneous crosslinker density) [38,39]. However, for a detailed study of inhomogeneous microgels, scattering techniques are stretched to their limits.

Scanning transmission soft x-ray microspectroscopy (STXM) is a powerful technique for high-contrast imaging of soft matter specimens due to resonant imaging [40]. Employing modern zone plate technology resolutions of 10 nm are accessible [41,42]. Although STXM is limited to rather thin specimens with sufficient transparency, the low absorption of water for photon energies below 530 eV has been successfully employed for in-situ investigations of various polymer particles in aqueous solution, e.g., gas filled microspheres [43,44], microcontainers [45,46], temperature-dependent phase-change microcapsules [47] or pH-sensitive polyvinyl composite microgels [48]. Recent advances resulted in 3D representations of nanoparticle coated microspheres from STXM focal series by means of a digital reconstruction algorithm [49]. The high penetration depth of soft x-rays in water is especially advantageous compared to electron microscopy.

In this paper we report on the microscopic characterization of isolated thermoresponsive poly(vinyl alcohol)/poly(methacrylate-*co*-*N*-isopropylacrylamide) (PMN-II) based microgel particles in aqueous environment. Aiming on a detailed structural analysis we recorded STXM micrographs and generated quantitative radial profiles of isolated microgel particles. A deconvolution model for rigid gas filled microspheres that respects the influence of the spherical particle geometry on the transmitted signal [50] was employed to monitor a temperature dependent decrease of the respective particle radius upon thermal treatment. Compared to conventionally used scattering techniques, direct imaging of individual particles provides the opportunity to derive the shrinking behaviour of differently sized particles. With the present study we are able to derive radial profiles that consist of a dense interior (“core”) and a less dense regime of dangling surface chains (“shell”). In addition, the comparison of larger and smaller particles indicates relative differences that can hardly be measured with other techniques.

2. Experimental

Thermoresponsive PMN-II microgel particles were synthesized via a water-in-water emulsion technique and cross-linked by photopolymerization according to a procedure described in detail elsewhere [51,52]. The effective amount of NIPAM incorporated in the network was 22% (w/w) and the average diameter of the particles was 2 µm according to scanning electron microscopy (dry state), DLS and confocal scanning laser microscopy (CLSM) in solution. The incorporation of NIPAM induces a thermoresponsive deswelling of the PVA-based microgel network above a VPTT of about 33 °C to achieve a new type of switchable microgels for drug transport [51]. An average chemical structure of the PMN-II network is depicted in Scheme 1.

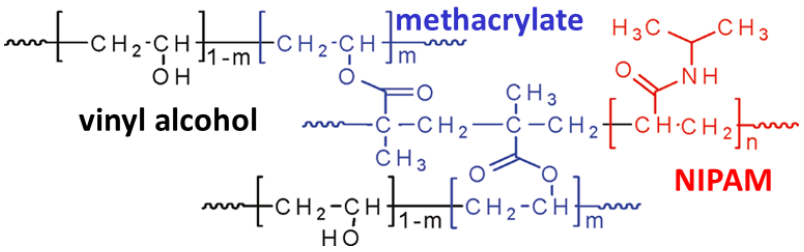

Scheme 1: Average structure of PMN-II network (m = 0.05; n= 0.12)

Liquid cells for in-situ STXM in aqueous environment were prepared by dropping the microgel solution on a 100 nm thin Si_3N_4-membrane (Silson Ltd., United Kingdom) and covering it with a second membrane. The resulting water microbasin was hermetically sealed with varnish [53]. To avoid absorption saturation by the aqueous environment only samples with water film thicknesses below 10 micrometers were used. The specimen temperature was controlled with a modified sample holder equipped with a heating resistor and a Pt 200 sensor [54].

STXM experiments were performed at the PolLux end station at the Swiss Light Source (SLS) [55]. The STXM setup uses synchrotron light from a bending magnet that is focused on the specimen by a Fresnel zone plate. The sample is raster-scanned through the first order focus spot of the zone plate with interferometric control while the transmitted photon intensity is recorded by a photomultiplier tube (Hamamatsu 647P) located behind the specimen. STXM images of isolated microgel particles were recorded at different temperatures with a dwell time of 1 or 2 ms and 520 eV incident photon energy. Within the so-called 'water window' (280 eV < hν < 525 eV) the absorption of carbon-containing material is larger than for water, thus offering significant image contrast. Radial transmission profiles of individual microgel particles (with ideal spherical shape) were extracted from the STXM images using the freely available analysis software aXis2000. The profiles were quantitatively analyzed in ROOT [56] by a least-square fitting analysis that takes a finite size of the focused x-ray beam into account (see supplementary information). We ensured that the observed effects were not affected by x-ray irradiation and that the temperature behavior was fully reversible.

3. Quantitative 3D analysis from 2D radial profiles

The transmitted intensity of monochromatic x-rays through matter (consisting of one chemical component) is described by the Lambert-Beer law:

$$I_t(x,y) = I_0 \exp(-\mu(h\nu)\cdot\rho\cdot D(x,y)) = I_0\cdot\exp(k(h\nu)\cdot D(x,y)) \quad (1)$$

$I_t(x,y)$ represents the local transmitted intensity and I_0 the incident photon intensity. The mass absorption coefficient μ strongly depends on the photon energy hν thus reflecting the high chemical sensitivity in soft x-ray absorption. Density, local thickness and the absorption coefficient of the absorbing material are given by ρ, D(x,y) and k(hν), respectively. In multicomponent systems the image contrast is governed by the specific absorption coefficients. In particular for heterogeneous soft matter samples, the tuneable photon energy enables optimum contrast imaging due to spectroscopic contrast [40].

To facilitate a quantitative analysis the local transmittance $I_t(x,y)$ from the 2D STXM micrographs of isolated microgel particles is transferred to a radial dependence I(r) by extraction of radial profiles. The geometrical model of the particles is adopted from a previous study of gas-filled microspheres [50]. The analysis is based on eq. (1) considering ideal spherical core-shell particles with an outer radius R_1 (cf. Fig. 1). We describe the particles by a homogenous interior (core) with radius R_0 and absorption parameter k_{core} (corresponding to region III, Fig. 1) and a (less dense) shell regime (region II) of thickness $h = R_1 - R_0$ with absorption parameter k_{shell} ($k_{shell} < k_{core}$). The shell corresponds to the dangling surface chains of the cross-linked polymer framework. The absorption of the surrounding water matrix is considered by an additional absorption coefficient k_{H2O} (region I). Note that the water film thickness exceeding the particle diameter ($d > 2\ R_1$) only contributes with a small homogenous background that is to be considered in the quantitative analysis. The additional water in the wet-cell as well as the two Si_3N_4 membranes absorbs a constant fraction of the transmitted intensity and is taken into account in I_0 which is also a fitting parameter.

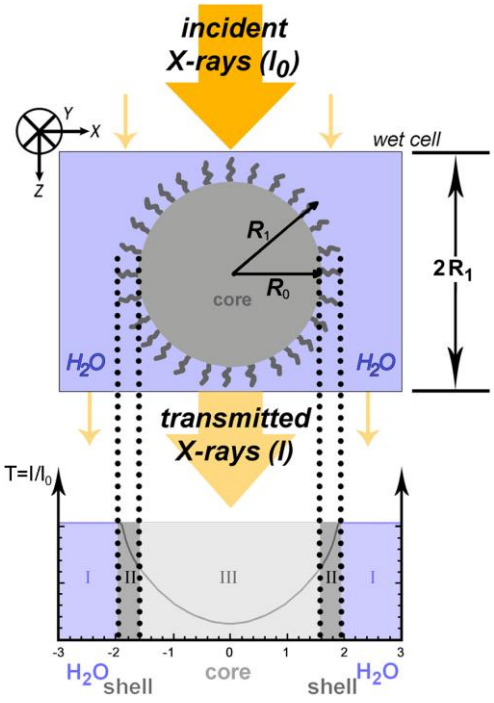

Fig. 1: Top: Schematic model of a spherical microgel particle consisting of a homogenous interior sphere and homogenous particle shell in aqueous surrounding with respective absorption coefficients defining the different radial regimes and variables. Bottom: radial

transmission profile and its behaviour in different regimes assuming low absorption of the water matrix (regime I).

Fig. 1 shows the generation of a transmission profile from a spherical microgel particle by convolution. The three regimes (water, shell and core) each are described by equations that include the respective absorption coefficients and component thicknesses. The latter parameters are derived from geometrical considerations. In the present model the mass absorption coefficient μ_i and density ρ_i in the respective regimes are constant and can therefore be replaced by the absorption coefficients k_i. For simplicity, the photon energy dependence of μ and k are neglected. We can thus derive the following equations for the 3 different regimes:

Regime I (H_2O), i.e. $|r| > R_1$:

$$I_t = I_0 \cdot \exp\{-k_{H2O} \cdot D_{H2O}\} = I_0 \cdot \exp\{-k_{H2O} \cdot 2R_1\} \quad (2a)$$

with $D_{H2O} = 2 \cdot R_1$ (2b)

Regime II (shell), i.e. $R_0 < |r| \leq R_1$:

$$I_t = I_0 \cdot \exp\{-k_{H2O} \cdot D_{H2O} - k_{shell} \cdot D_{shell}\} \quad (3a)$$

with $D_{H2O} = 2 \cdot R_1 - 2 \cdot \sqrt{R_1^2 - r^2}$ and $D_{shell} = 2 \cdot \sqrt{R_1^2 - r^2}$ (3b)

Regime III, i.e. $|r| \leq R_0$:

$$I_t = I_0 \cdot \exp\{-k_{H2O} \cdot D_{H2O} - k_{shell} \cdot D_{shell} - k_{core} \cdot D_{core}\} \quad (4a)$$

with $D_{H2O} = 2 \cdot R_1 - 2 \cdot \sqrt{R_1^2 - r^2}$; $D_{shell} = 2 \cdot \sqrt{R_1^2 - r^2} - 2 \cdot \sqrt{R_0^2 - r^2}$

and $D_{core} = \sqrt{R_0^2 - r^2}$ (4b)

For the quantitative analysis we consider continuity at the regime borders shell/water ($r = R_1$) and shell/core ($r = R_0$). Equations 2 – 4 are used for a least-square fit procedure. k_{H2O} was kept constant during the iterative process at a value of 0.11 μm^{-1} in accordance with previous studies [50].

4. Results and discussion

Fig. 2 shows the STXM micrographs of two PMN-II microgel particles in aqueous environment recorded at three different temperatures. During the heating of the specimen the microgel particles show deswelling as expected from their thermoresponsive behavior. Positional changes due to thermal drift were corrected. Note that the stated temperatures are those recorded about 6 mm away from the wet cell sample. While the starting temperature (T_1 = 25°C) was measured with high accuracy, we may conclude that the actual sample tem-

peratures for 45°C (T_2) and 55°C (T_3) measurements are lower and therefore closer to the VPTT of PNIPAM. The smaller features close to the investigated particles are either very small microspheres or residuals from the polymerization educts from the solution. However, they are irrelevant for the quantitative analysis since they do not affect the radial profile extraction from the 2D images.

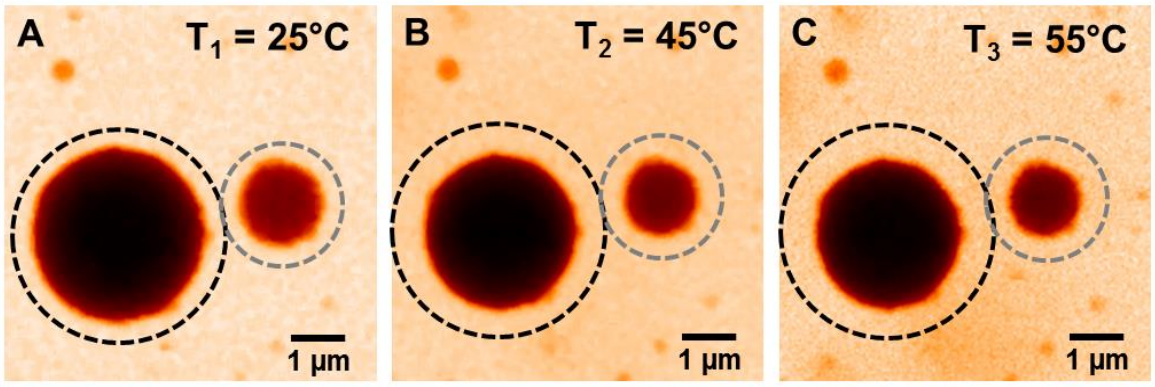

Fig. 2: STXM micrographs of two spherical microgel (PMN-II) particles at temperatures of 25°C (A), 45°C (B) and 55°C (C). The dotted circles indicate the borders of the respective extracted radial profiles. The images were recorded at $h\nu$ = 520 eV to prevent absorption saturation by the surrounding water.

The dark dotted circles in Fig. 2 depict the regions that have been defined to extract the respective radial profiles. The resulting profiles for the two representative particles are shown in Fig. 3. Upon heating a reduction in radial size is obvious for both particles and simultaneously the transmitted intensity I_t is decreasing. Since the experiment is performed at 520 eV, the absorption of water does not significantly contribute to the absorption. In contrast, the reduction of I_t is due to stronger absorption within the particle, i.e., higher density and therefore increased optical density upon the release of water. For both particles we observe some minor changes in their diameters upon heating from 45°C to 55°C, which is some indication that the particles have not yet reached the state of complete deswelling at 45°C.

Fig. 3 summarizes the graphic result of the least-square fit analysis of the radial profiles for the larger (Fig. 3A) and smaller particle (Fig. 3B) in the micrographs depicted in Fig. 2. For smaller radii, the radial profiles are well represented by the applied model while for larger radii the fitted curves slightly deviate from the experimental data. In particular for $|r| < 0.5$ nm the radial profile of the larger particle has no pronounced curvature, but appears flat suggesting a constant absorption. The explanation for this finding is related to the overall thickness of the particle interior. Typically, STXM uses resonant excitation for maximum image contrast and thus, absorption saturation often occurs for film thicknesses of about 200 nm. Using non-resonant excitation as in the present case ($h\nu$ = 520 eV), the calculated penetration depth for carbon is around 680 nm. Therefore, absorption saturation plays a significant role in the case of larger particles, while for the smaller particle, the experimental curve follows the model (eqns. 4a, 4b) within the shell and core regime. However, for both microgel particles the flanks of the radial profiles are well represented by the quantitative fits and the deviations are restricted to $|r| < R_0$. Therefore, the determination of the core-shell

border will not be affected and the absorption coefficients just to a small extent. The respective fit results for R_0, R_1, k_{core} and k_{shell} are denoted in detail in the supplementary.

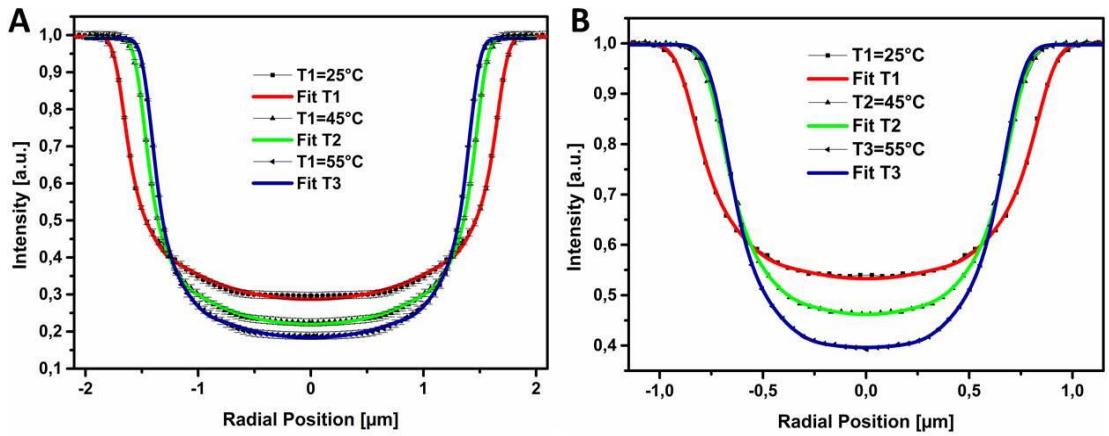

Fig. 3: Least-square fit analysis of the temperature dependent radial profiles for the larger (A) and smaller particle (B), respectively, according to eqns. 3 and 4.

The temperature dependent behaviour of the selected PMN-II microgel particle diameters is illustrated in Fig. 4. Upon heating the inner radius R_0 changes for the larger particle by approximately 30% from T_1 to T_3 ($T_1 \rightarrow T_2$: 15.5% decrease, $T_2 \rightarrow T_3$: 16.3% decrease) while the outer radius R_1 decreases by 15.0 % (-11.0 % and -4.4 % for the respective temperature steps). For the smaller particle the situation was comparable: a 42.7% overall decrease for R_0 during heating from T_1 to T_3 ($T_1 \rightarrow T_2$: 22.6% decrease, $T_2 \rightarrow T_3$: 25.9% decrease), and 18.5% decrease for R_1 (-15.8% / -3.2%). Simultaneously the respective k values are increasing by about 25% in both regimes for heating from T_1 to T_2 and by 50% from T_1 to T_3. Since a lower particle diameter goes along with decreasing x-ray penetrated specimen volume, this finding detects a strong increase in material density. Considering the overall particle diameter, these findings are in accordance with a previous study based on scattering data (dynamic light scattering, neutron scattering) and confocal laser scanning microscopy [52]. However, according to our results, the particle shrinkage is mainly governed by a deswelling of the highly cross-linked core network. The diameter of the shell ($R_1 - R_0$) is found to be relatively constant, while this regime also shows a strong increase of polymer density that goes along with solvent release.

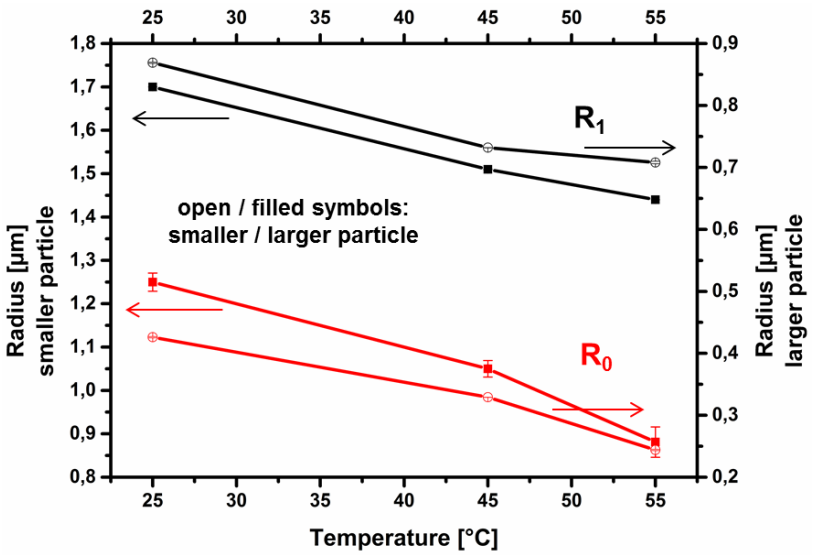

Fig. 4: Temperature-dependent change of the particle radii of two differently sized PMN-II microgel particles.

5. Conclusions and Outlook

Due to their significant PNIPAM content PMN-II microgel particles show significant deswelling and water release upon heating above the VPTT. Quantitative fitting of radial profiles extracted from *in-situ* recorded high-resolution STXM micrographs allows for a detailed analysis of this shrinking for individual particles of different size and / or density. It should be mentioned that the presented approach presents an elegant way to achieve information of the 3D shape of the investigated specimen from pure 2D data.

The accordance of the model with the experimental data supports our approach for the quantitative analysis based on the projected radial profiles. Although some deviations from ideal profiles occur for larger particles due to absorption saturation, we obtain valuable insight into the structural modifications in microgel particles induced by the temperature increase. Based on the derived fit parameters for the two exemplary particles, we are able to confirm the increase in (optical) density in the interior of the particles due to the release of water upon temperature increase above VPTT. This is already obvious from the reduction of intensity in the radial profiles for $|r| \approx 0$. Quantification indicates a pronounced increase for k_{core} for either size. Furthermore, we find no significant shrinkage of the shell regime representing dangling surface chains of the polymer network. This finding is rather surprising, since usually a collapse of this regime is considered in literature [50].

In summary, STXM microanalysis of individual thermoresponsive microgel particles in water allows detailed insight into the morphology changes. Although the model for the radial profile is only based on simple geometric considerations, we are able to observe structural variations with high accuracies. The derived values are in agreement with complementary studies on the same material. Further model studies will take into account potential concentration gradients in the shell regime to obtain a more detailed insight into radial water gradients in the less dense material. This will require additional experiments in the C1s and O1s photon energy regime to increase chemical sensitivity beyond pure mass absorption.

Acknowledgements

We gratefully acknowledge experimental support by Dr. J. Raabe from the PolLux beamline at the Swiss Light Source (SLS). We thank B. Rösner (FAU Erlangen-Nürnberg) for fruitful discussions. The project was funded by the Bundesminister für Bildung und Forschung, contract 05 K10WEA. The research leading to these results has received funding from the European Community's Seventh Framework Programme (FP7/2007-2013) under grant agreement n.312284 (CALIPSO). A.S. acknowledges funding through the Graduate School Molecular Science (GSMS).

References:

[1] W.O. Baker, *Ind. Eng. Chem.*, **1949**, 41, 511-510.
[2] R.H. Pelton, P. Chibante, *Colloids Surf.*, **1986**, 20, 247-256.
[3] B.R. Saunders, B. Vincent, *Adv. Colloid Interface Sci.*, **1999**, 80, 1-25.

[4] N. Sanson, J. Rieger, *Polym. Chem.*, **2010**, 1, 965-977.
[5] J.M. Weissman, H.B. Sunkara, A.S. Tse, S.A. Asher, *Science*, **1996**, 274, 959-960.
[6] R.H. Pelton, *Adv. Colloid Interface Sci.*, **2000**, 85, 1-33.
[7] M. Karg, T. Hellweg, *Curr. Opin. Colloid Interface Sci.*, **2009**, 14, 438-450.
[8] L.A. Lyon, A. Fernandez-Nieves, *Annu. Rev. Phys. Chem.*, **2012**, 63, 25-43.
[9] T. Tanaka, S. Ishiwata, C. Ishimoto, *Phys. Rev. Lett*., **1977**, 38(14), 771-774.
[10] T. Tanaka, *Phys. Rev. Lett.*, **1978**, 40(12), 820-823.
[11] T. Hoare, R. Pelton, *Macromolecules*, **2004**, 37, 2544-2550.
[12] L. Bromberg, M. Temchenko, T.A. Hatton, *Langmuir*, **2002**, 18, 4944-4952.
[13] D. Schmaljohann, *Adv. Drug Del. Rev.*, **2006**, 58(15), 1655-1670.
[14] T.R. Hoare, D.S. Kohane, *Polymer*, **2008**, 49, 1993-2007.
[15] Y. Guan, Y. Zhang, *Soft Matter*, **2011**, 7(14), 6375-6385.
[16] R.F.S. Freitas, E.L. Cussler, *Chem. Eng. Sci.*, **1987**, 42(1), 97-103.
[17] S. Höfl, L. Zitzler, T. Hellweg, S. Herminghaus, F. Mugele, *Polymer*, **2007**, 48(1), 245-254.
[18] G.R. Hendrickson, L.A. Lyon, *Soft Matter*, **2009**, 5(1), 29-35.
[19] M.R. Islam, M.J. Serpe, *Chem. Comm.*, **2013**, 49(26), 2646-2648.
[20] H. Kawaguchi, K. Fujimoto, Y. Mizuhara, *Colloid Poly. Sci.*, **1992**, 270, 53-57.
[21] B. Jeong, A. Gutowska, *Trends Biotechnol.*, **2002**, 20(7), 305-311.
[22] X. Zhu, X. Gu, L. Zhang, X.-Z. Kong, *Nanoscale Res. Lett.*, **2012**, 7, 519.
[23] S. Nayak, L.A. Lyon, *Angew. Chem. Int. Ed.*, **2005**, 44, 7686-7708.
[24] P. Schexnailder, G. Schmidt, *Colloid Polym. Sci.*, **2009**, 287(1), 1-11.
[25] D.M. Han, Q.M. Zhang, M.J. Serpe, *Nanoscale*, **2015**, 7(6), 2784-2789.
[26] W. McPhee, K.C. Tam, R. Pelton, *J. Colloid Interface Sci.*, **1993**, 156, 24-30.
[27] A. Fernández-Nieves, M. Márquez, *J. Chem. Phys.*, **2005**, 122, 084702.
[28] M. Heskins, J.E. Guillet, *J. Macromol. Sci. Chem.*, **1968**, 2(8), 1441-1455.
[29] K. Kratz, T. Hellweg, W. Eimer, *Polymer*, **2001**, 42, 6631-6639.
[30] J. Wu, B. Zhou, Z. Hu, *Phys. Rev. Lett.*, **2003**, 90(4), 048304.
[31] P.J. Yunker, K. Chen, M.D. Gratale, M.A. Lohr, T. Still, A.G. Yodh, *Rep. Prog. Phys.*, **2014**, 77, 056601.
[32] Y.H. Bae, T. Okano, S.W. Kim, *J. Polym. Sci. B*, **1990**, 28(6), 923-936.
[33] R.H. Pelton, *J. Colloid Interface Sci.*, **2010**, 348(2), 673-674.
[34] C.D. Jones, M.J. Serpe, L. Schroeder, L.A. Lyon, *J. Am. Chem. Soc.*, **2003**, 125, 5292-5293.
[35] S. Wongsuwarn, D. Vigolo, R. Cerbino, A.M. Howe, A. Vailati, R. Piazza, P. Cicuta, *Soft Matter*, **2012**, 8(21), 5857-5863.
[36] A. Koniger, N. Plack, W. Kohler, M. Siebenburger, M. Ballauff, *Soft Matter*, **2013**, 9(5), 1418-1421.
[37] B.R. Saunders, *Langmuir*, **2004**, 20(10), 3925-3932.
[38] R. Acciaro, T. Gilányi, I. Varga, *Langmuir*, **2011**, 27(12), 7917-7925.
[39] T. Still, K. Chen, A.M. Alsayed, K.P. Aptowicz, A.G. Yodh, *J. Colloid Interface Sci.*, **2013**, 405, 96-102.
[40] H. Ade, A.P. Hitchcock, *Polymer*, 2008, 49, 643-675.
[41] J. Vila-Comamala, K. Jefimovs, J. Raabe, T. Pilvi, R.H. Fink, M. Senoner, A. Maassdorf, M. Ritala, C. David, *Ultramicroscopy*, **2009**, 109, 1360-1364.
[42] W. Chao, P. Fischer, T. Tyliszczak, S. Rekawa, E. Anderson, P. Naulleau, *Opt. Express*, **2012**, 20, 9777-9783.
[43] G. Tzvetkov, B. Graf, P. Fernandes, A. Fery, F. Cavalieri, G. Paradossi, R.H. Fink, *Soft Matter*, **2008**, 4, 510-514.
[44] G. Tzvetkov, A. Späth, R.H. Fink, *Radiat. Phys. Chem.*, **2014**, 103, 84-88.

[45] C. Déjugnat, K. Köhler, M. Dubois, G.B. Sukhorurov, H. Möhwald, T. Zemb, P. Guttmann, *Adv. Mater.*, **2007**, 19, 1331-1336.
[46] A. Späth, H. Minami, T. Suzuki, R.H. Fink, *RSC Adv.*, **2014**, 4, 3272-3277.
[47] G. Tzvetkov, B. Graf, R. Wiegner, J. Raabe, C. Quitmann, R. Fink, *Micron*, **2008**, 39, 275-279.
[48] S. Fujii, S.P. Armes, T. Araki, H. Ade, *J. Am. Chem. Soc.*, **2005**, 127(48), 16808-16809.
[49] A. Späth, S. Schöll, C. Riess, D. Schmidtel, G. Paradossi, J. Raabe, J. Hornegger, R.H. Fink, *Ultramicroscopy*, **2014**, 144, 19-25.
[50] P.A.L. Fernandes, G. Tzvetkov, R.H. Fink, G. Paradossi, A. Fery, *Langmuir*, **2008**, 24, 13677-13682.
[51] S.V. Ghugare, P. Mozetic, G. Paradossi, *Biomacromolecules*, **2009**, 10(6), 1589-1596.
[52] S.V. Ghugare, E. Chiessi, R. Fink, Y. Gerelli, A. Scotti, A. Deriu, G. Carrot, G. Paradossi, *Macromolecules*, **2011**, 44(11), 4470-4478.
[53] B. Graf-Zeiler, G. Tzvetkov, R.H. Fink, *Chem. Phys. Chem.*, **2011**, 12(18), 3503-3509.
[54] G. Tzvetkov, R.H. Fink, *Scripta Mater.*, **2008**, 59, 348-351.
[55] J. Raabe, G. Tzvetkov, U. Flechsig, M. Böge, A. Jaggi, B. Sarafimov, M.G.C. Vernooij, T. Huthwelker, H. Ade, D. Kilcoyne, T. Tyliszczak, R.H. Fink, C. Quitmann, *Rev. Sci. Instrum.*, **2008**, 79, 113704.
[56] R. Brun, F. Rademakers, *Nucl. Instrum. Meth. A*, **1997**, 389, 81-86.